Earth and Planetary Science Letters 297 (2010) 633–645

Contents lists available at ScienceDirect

Earth and Planetary Science Letters

journal homepage: www.elsevier.com/locate/epsl

Early Jurassic shale chemostratigraphy and U–Pb ages from the Neuquén Basin (Argentina): Implications for the Toarcian Oceanic Anoxic Event

Adriano Mazzini [a,*], Henrik Svensen [a], Héctor A. Leanza [b], Fernando Corfu [c], Sverre Planke [a,d]

[a] Physics of Geological Processes, University of Oslo, Sem Sælandsvei 24, Box 1048, 0316 Oslo, Norway
[b] Servicio Geologico Minero Argentino y CONICET, 1322 Buenos Aires, Argentina
[c] Department of Geosciences, University of Oslo, PO Box 1047 Blindern, 0316 Oslo, Norway
[d] Volcanic Basin Petroleum Research (VBPR), Oslo Research Park, 0349 Oslo, Norway

ARTICLE INFO

Article history:
Received 11 December 2009
Received in revised form 5 July 2010
Accepted 7 July 2010
Available online 9 August 2010

Editor: R.W. Carlson

Keywords:
Toarcian Oceanic Anoxic Event
Neuquén Basin
carbon isotopes
tuff layers
zircon U–Pb dating
Karoo Basin

ABSTRACT

New data from a Lower Jurassic shale section in the Neuquén Basin, Argentina, are presented in order to better constrain the triggering mechanism for the Toarcian Oceanic Anoxic Event (TOAE) and the associated negative carbon isotope excursion. Chemostratigraphy from a 65 m thick shale-dominated marine section of Late Pliensbachian to Early Toarcian age shows the presence of a 19.5 m thick interval of organic-rich black shale where the bulk rock organic carbon content reaches almost 4 wt.%. The $\delta^{13}C$ of the bulk organic matter changes from −22.3‰ in the lower parts of the profile to −29.8‰ VPDB in the black shale interval, documenting a −8‰ excursion over five stratigraphic meters. Twelve interbedded tuff layers, representing fallouts from paleo-Andean arc magmatism, were discovered in the section. Dating by ID-TIMS of zircons from two tuff beds located within the carbon isotope excursion interval gave ages of 181.42 ± 0.24 Ma and 180.59 ± 0.43 Ma. Assuming linear sedimentation rates within the black shale interval, the initiation of the anoxic event occurred at 182.16 ± 0.6 Ma, lasting until 180.16 ± 0.66 Ma. Thus the total duration is between 0.74 and 3.26 Ma, taking into account the propagation of dating uncertainties. This also allowed to obtain a new and improved estimate of the Pliensbachian–Toarcian boundary. The U/Pb age of the initiation of the observed carbon isotope excursion overlaps the U/Pb emplacement ages of mafic sill intrusions in the Karoo Basin in South Africa, and supports the hypothesis that thermogenic methane released during contact metamorphism within the Karoo Basin was the main trigger of the anoxic event. Our findings show that the Toarcian carbon isotope excursion is present also in the southern hemisphere and that the TOAE was a global phenomenon likely triggered by a massive greenhouse gas release.

1. Introduction

The Toarcian Stage of the Lower Jurassic is characterized by a pronounced negative carbon isotope excursion (CIE) in organic-rich marine sediments, deposited during an oceanic anoxic event (OAE) (Jenkyns, 1988). Several hypotheses have been proposed to explain these observations and geochemical signatures, including local processes [Tethys anoxia, stagnant oceanic basins (Küspert, 1982; McArthur et al., 2000; Schouten et al., 2000; van de Schootbrugge et al., 2005; Wignall et al., 2005, 2006; Mattioli et al., 2008; McArthur et al., 2008)], and global processes [e.g. gas release from either gas hydrates or contact metamorphosed organic-rich sediments (Hesselbo et al., 2000; Svensen et al., 2004; Kemp et al., 2005; McElwain et al., 2005; Hesselbo et al., 2007; Svensen et al., 2007; Hermoso et al., 2009)] (see Cohen et al., 2007 and references therein for a broad discussion).

The sections studied by these authors include Early Toarcian shales and limestones from marine depositional systems that show negative CIE. If the carbon isotope excursion represents a global carbon cycle perturbation derived from carbon degassing (i.e. methane and carbon dioxide), it likely led to a global warming. Despite the fact that the Toarcian OAE (TOAE) is considered to be widespread, the main investigated localities are from western Europe and include mostly Boreal epicontinental seaway locations.

Identification of a unique geological mechanism for gas release during the Toarcian would strengthen the hypothesis that the event was global and related to greenhouse gas release. Contact metamorphism of organic-rich shale followed by degassing of methane to the atmosphere has been proposed to be responsible for the Toarcian event (Svensen et al., 2004), and is supported by geological evidence from the Karoo Basin (Svensen et al., 2007) and Antarctica (McElwain et al., 2005). The link between the Karoo large igneous province (LIP) and the TOAE, however, is still not fully understood since the timing of sill emplacement and the timing of the isotope excursion cannot be directly compared.

In order to test this hypothesis we have studied Pliensbachian and Toarcian shales and dated previously unknown interbedded volcanic

* Corresponding author.
E-mail address: adriano.mazzini@fys.uio.no (A. Mazzini).

0012-821X/$ – see front matter © 2010 Elsevier B.V. All rights reserved.
doi:10.1016/j.epsl.2010.07.017

tuff layers outcropping in Argentina (Neuquén Basin, Mendoza province) (Fig. 1). South America is the ideal target for testing the potential link between the Karoo–Ferrar igneous province and the origin of the carbon isotope excursion recorded in the Toarcian sediments. The palaeogeographical record shows that during the Lower Jurassic both South America and South Africa were part of the Gondwana continent (Fig. 2) but their initial scission and the formation of the Neuquén Basin also occurred at this time (Fig. 3). The aims of this project are to establish a chemostratigraphic record spanning the Pliensbachian and Toarcian of the Neuquén Basin, identifying the negative CIE, if present, and to obtain high quality U/Pb ages from the tuffs in order to directly compare zircon ages of the carbon isotope excursion with zircon ages of the sill intrusions (hence carbon degassing) in the Karoo Basin.

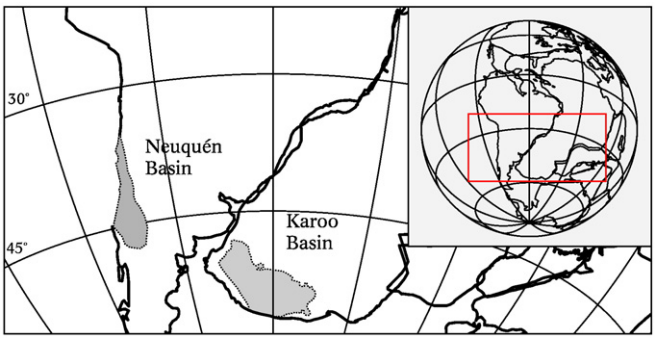

Fig. 2. Palaeogeography of South America and Africa at about 180 Ma (Toarcian) with the Neuquén and Karoo basins shown in grey.

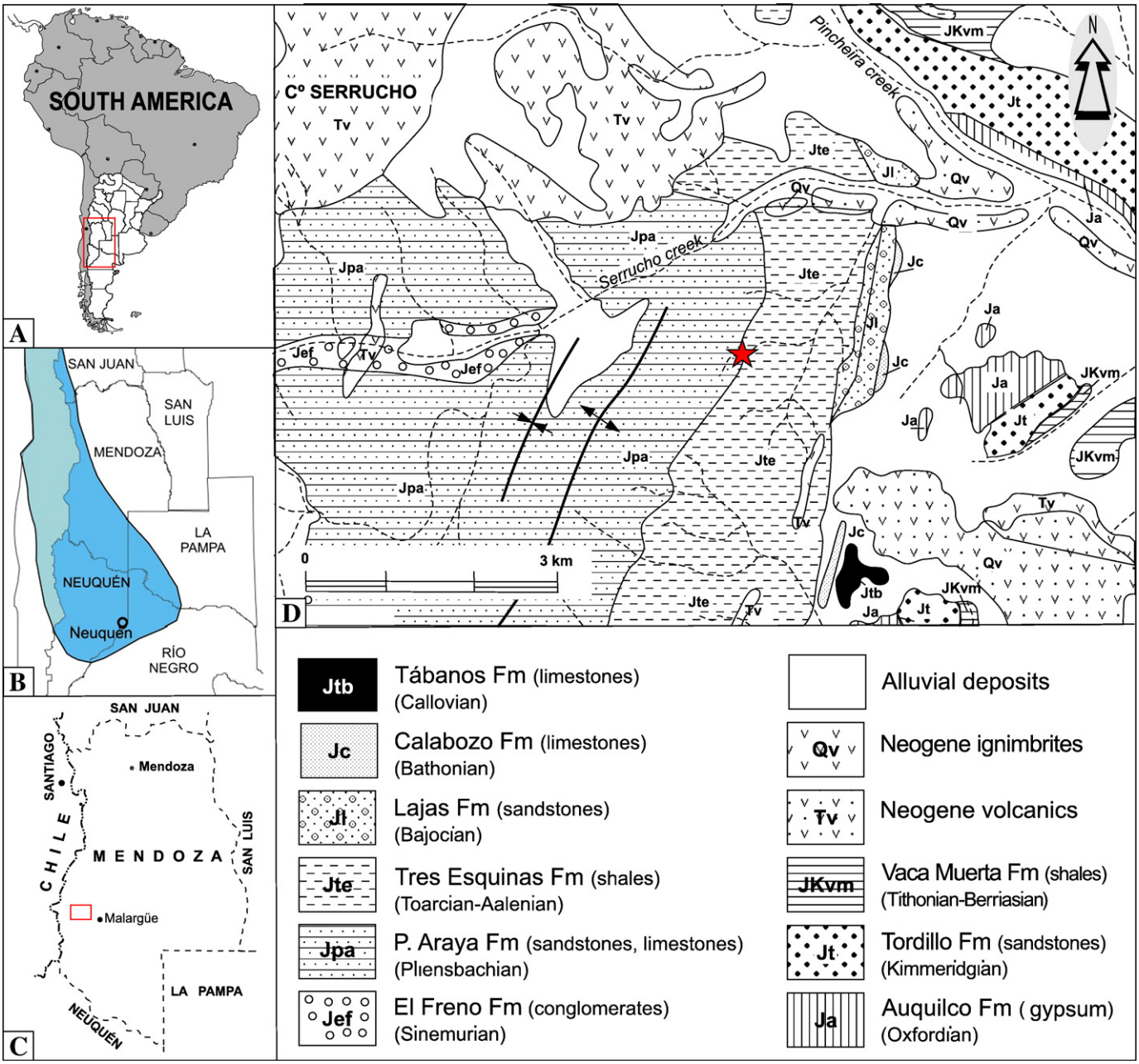

Fig. 1. Location map of the Neuquén Basin and the studied area. A) The Neuquén Basin in South America; B) Actual position of the Neuquén Basin in west central Argentina and central Chile; C) Mendoza province, showing the position of the logged section; and D) Geological sketch of the Serrucho Creek area (after Gulisano and Gutiérrez Pleimling, 1995), showing the logged area (star) and lithostratigraphic units with main lithologies and ages.

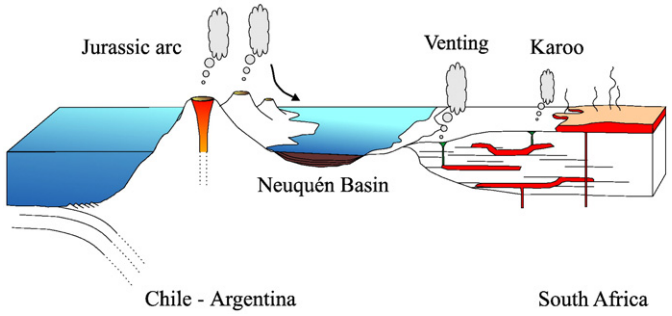

Fig. 3. Cartoon (not to scale) of the geological setting during the Lower Toarcian. During the initial spreading of Pangea, South Africa and Chile–Argentina were separated by the Neuquén Basin where anoxic sediments were deposited. The tuff layers are derived from Jurassic arc volcanism in the west.

2. Geological setting

2.1. The Neuquén Basin

The Neuquén Basin is located in the central part of western Argentina and eastern Chile between latitudes 34° and 41° S in the provinces of Neuquén, Mendoza, Río Negro and La Pampa (Fig. 1). It extends northwards along the axis of the Andean Cordillera up to 31° S (San Juan province), where it is called the Aconcagua Basin. Between 34° and 37° S it is restricted to the Cordilleran belt as a narrow N–S elongated strip. South of 37° S it broadens eastwards, into an extra-Andean domain, where it is known as the Neuquén Embayment.

The Neuquén Basin (Fig. 2) is a Mesozoic back-arc rift basin located on the western convergent margin of the South America plate (Uliana and Biddle, 1988; Legarreta and Uliana, 1999; Ramos, 2009). The infill of the Neuquén Basin exceeds 7000 m of marine and continental sedimentary rocks (epiclastics, carbonates, evaporites and pyroclastics) which range in age from Late Triassic to the Paleocene.

The Neuquén Basin formed during the fragmentation of Gondwana and the subsequent opening of the South Atlantic Ocean (Fig. 2). In the Triassic and Early Jurassic a series of halfgrabens trending NNW–ESE formed and were filled by volcanic and sedimentary sequences (the Precuyano cycle) at separate depocentres (Atuel, La Valenciana, Cordillera del Viento, Chachil) (Gulisano et al., 1984). The rifting stage was followed by an Early Jurassic widespread marine ingression from the Panthalassic Ocean, thus changing from localized rifting to a generalized subsidence (Legarreta and Gulisano, 1989; Vergani et al., 1995; Legarreta and Uliana, 1999). As a result, these depocentres, located to the east of the arc and trench system, became progressively inter-connected, and were integrated during Pliensbachian times into an extensive area of marine sediment deposition located between the volcanic arc to the west and the South American foreland to the east. The expansion of a broader basin coincided with the initiation of a long-term stage of subsidence, during which a number of marine units ascribed to the Cuyo Group were deposited (Groeber, 1946; Gulisano et al., 1984).

The Neuquén Basin maintained an almost continuous subsidence rate until the Paleocene (Legarreta and Gulisano, 1989), although local episodes of uplift, folding, erosion, and evidence of synsedimentary tectonics are recorded (Ramos, 1988). After that, a stage of uplift and non-deposition (Eocene hiatus) was followed by compressional tectonics during the Oligocene to the Late Miocene, and the basin reached its current structural configuration (Ramos, 2000).

2.2. Geology of the Serrucho Creek area

The outcrops chosen for this study are located in the Serrucho Creek in southern Mendoza, and belong to the La Valenciana depocentre (Giambiagi et al., 2005). They include mixed marine and non marine formations (El Freno, Puesto Araya, Tres Esquinas, Lajas, Calabozo and Tábanos) of the Cuyo Group (Sinemurian to Early Callovian), as well as Mesozoic and Cenozoic strata (Fig. 1). The uppermost Puesto Araya (carbonates, shales) and the lowermost Tres Esquinas formations (shales, sandstones) are present in the studied section (Fig. 4A) Previous important biostratigraphic studies, using ammonites, bivalves and brachiopod zones and assemblages compared with the European Standard zones and other regions of the world, show that Late Pliensbachian and Early Toarcian sediments outcrop at the Serrucho Creek locality (Stipanicic, 1969; Riccardi, 1984; Damborenea, 1987; Manceñido, 1990; Riccardi et al., 1990; Damborenea et al., 1992; Riccardi et al., 2000; Riccardi, 2008).

The Puesto Araya Formation (Volkheimer, 1978) has been divided in two parts (Giambiagi et al., 2008): the lower Puesto Araya Formation (Middle Hettangian–Sinemurian) with fan-deltaic sediments (Lanés, 2005), and the upper Puesto Araya Formation (late Early Sinemurian–Late Pliensbachian) with transgressive storm-dominated and carbonate-rich platform sediments deposited during the initial stage of basin subsidence. Valencio et al. (2005) presented a first chemostratigraphy study of the Puesto Araya Formation based on carbon isotopic results on the bivalves *Weyla* and *Gryphaea* present in this unit.

The Tres Esquinas Formation (Stipanicic, 1969) is regionally equivalent in the Neuquén province to the Los Molles Formation (Weaver, 1931). In the Serrucho Creek area, the Tres Esquinas Formation (~380 m thick) ranges in age from the Early Toarcian to the Late Bajocian; it overlies the Puesto Araya Formation and is capped by the Lajas Formation (Gulisano and Gutiérrez Pleimling, 1995). The basal portion of the Tres Esquinas Formation consists of organic-rich black shales (Figs. 4C, D), locally interbedded with carbonaceous siltstones and sporadic tuff layers (Fig. 4E). Although no specific palaeobathymetric studies were made in this lower section, our fossil and lithological observations in the field suggest that it belongs to outer shelf deposits in which the water column was not deeper than 200 m (Gulisano and Gutiérrez Pleimling, 1995). Above the basal portion of this unit, the shales are dark grey in colour and are interbedded with carbonaceous siltstones, representing outer shelf to basinal facies. Further up in the formation, a more active depositional system is present with a series of event beds thought to be of turbidite or traction current origin that deposited arenaceous units which alternate hemipelagic fine grained sediments. As a result of a sudden sea level fall in the Late Bajocian, the sandy fluvio-estuarine facies of the prograding Lajas Formation result in the sharp upper boundary of the Tres Esquinas Formation (Gulisano and Gutiérrez Pleimling, 1995).

3. Materials and methods

3.1. Field work

Exploratory field work in the Neuquén Basin was carried out in 2005 and later during March–April 2008. After a regional reconnaissance conducted to locate good outcrops of Early Jurassic strata and interbedded tuff layers, the Serrucho Creek area to the west of Malargüe city was selected for a detailed logging and sampling campaign. A Thales navigation Mobile Mapper GPS was used to get precise coordinates of sampling locations. The logged section is 127.5 m thick and includes the uppermost 6.5 m of the Puesto Araya Formation and the lowermost 121 m of the Tres Esquinas Formation (Figs. 1, 5). Identification of guide fossils was done in the field. Nineteen tuff layers were found and sampled for geochronological analyses through the 127.5 m of section. They range in thickness from 5–10 cm down to a few centimeters, and have the typical appearance of bentonites consisting mainly of white clay with weathered brownish surface exposures (Fig. 4E).

Fig. 4. Outcrops around the Serrucho Creek region, southern Mendoza province; (A) Uppermost limestones of the Puesto Araya Formation covered by black shales of the Tres Esquinas Fm.; in the background Auquilco gypsum outcrops along the Serrucho Creek valley; (B) Anoxic black shales above the Puesto Araya Formation with Lajas Formation outcropping in the background; (C) Contact between the Puesto Araya Formation and the Tres Esquinas Formation The thick limestone benches in the centre of the image define the lower boundary of the black shales; (D) Detail of the black shales along the creek showing the intercalation of silty and carbonate-rich layers in the shaly deposits; and (E) Tuff layer within the Tres Esquinas Formation ~22 m above the base of the section.

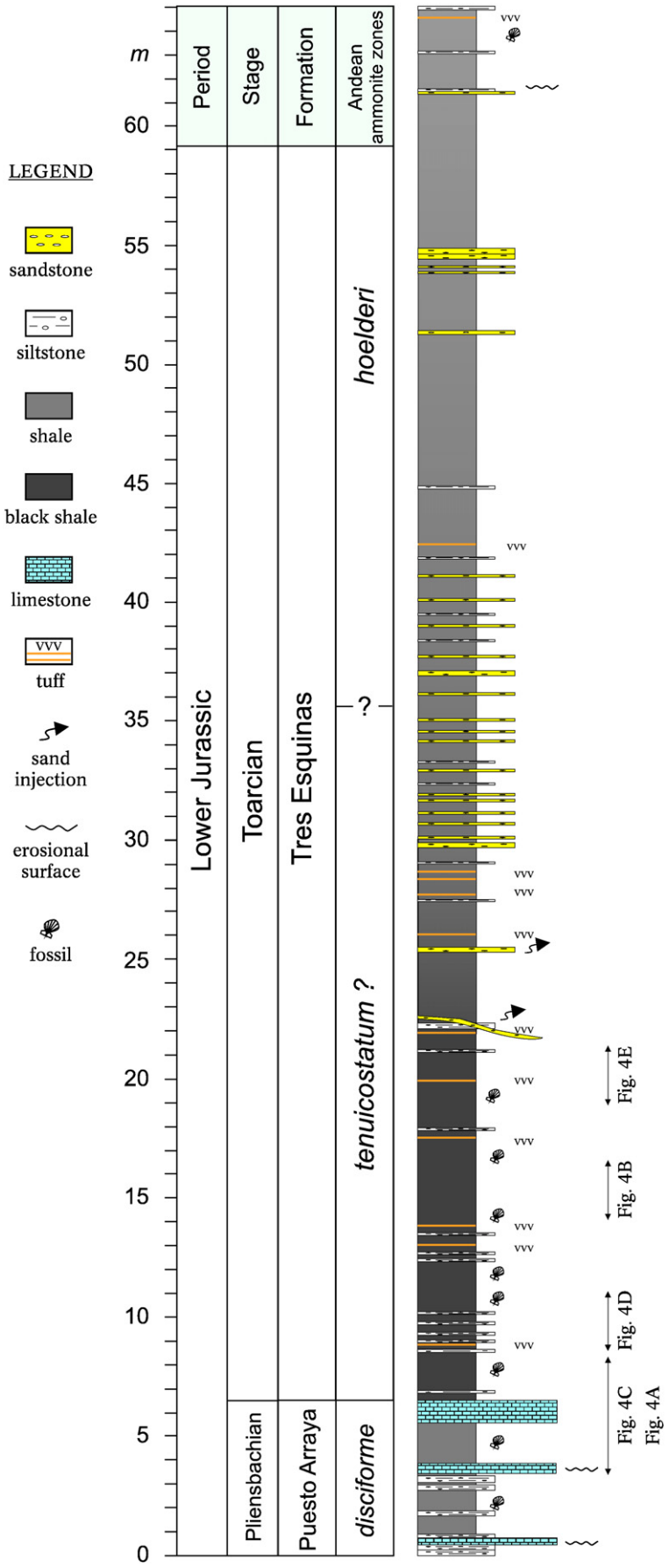

Fig. 5. Logged section highlighting the main lithological features, sedimentary structures, and ammonite zones. Ages are indicated based on fossil identifications.

Table 1
Sampling intervals, carbon isotope ratios, and TOC data.

Sample number	Depth (m)	Lithology	Comments	Organic C $\delta^{13}C_{VPDB}$		TOC wt. (%)	Vitrinite Ro (%)
				shale	carbonate-rich		
AR08AS60	61.4	Siltstone	More carbonate		-28.4	2.50	n.d.
AR08AS59	60.7	Shale		-26.6		2.03	n.d.
AR08AS58	57.8	Shale		-26.1		1.94	n.d.
AR08AS57	52.6	Shale		-26.4		1.93	n.d.
AR08AS56	50.2	Shale		-29.3		1.45	n.d.
AR08AS55	47.2	Shale		-26.4		2.33	n.d.
AR08AS54	44.8	Siltstone	More carbonate		-28.9	2.55	n.d.
AR08AS53	43.8	Shale		-27.0		1.28	n.d.
AR08AS52	42.4	Tuff?					n.d.
AR08AS51	41.8	Siltstone	More carbonate		-28.2	2.29	n.d.
AR08AS50	41.3	Shale		-26.8		2.48	n.d.
AR08AS49	40.5	Shale		-27.4		3.11	n.d.
AR08AS48	39.5	Siltstone			-26.3	2.94	n.d.
AR08AS47	37.9	Shale		-26.4		1.54	n.d.
AR08AS46	35.7	Shale		-25.4		1.31	n.d.
AR08AS45	33.9	Black shale		-27.0		3.62	n.d.
AR08AS44	32.4	Siltstone	More carbonate		-27.7	2.94	n.d.
AR08AS43	32.1	Black shale		-27.6		1.53	n.d.
AR08AS42	30.5	Black shale		-27.9		1.98	n.d.
AR08AS41	29.1	Siltstone	More carbonate		-29.4	2.29	n.d.
AR08AS40	28.8	Black shale		-27.2		2.53	n.d.
AR08AS39	28.7	Tuff					n.d.
AR08AS38	28.4	Tuff					n.d.
AR08AS37	27.8	Black shale		-28.1		1.57	n.d.
AR08AS36	27.7	Tuff					n.d.
AR08AS35	26.1	Black shale	End of excursion	-29.3		2.01	n.d.
AR08AS34	26.0	Tuff					n.d.
AR08AS33	25.4	Sandstone	Injected sand?				n.d.
AR08AS32	24.8	Black shale		-28.8		3.75	n.d.
AR08AS31	23.7	Black shale		-29.3		3.37	n.d.
AR08AS30	22.2	Siltstone			-29.7	2.71	n.d.
AR08AS29	21.9	Tuff					n.d.
AR08AS28	21.5	Black shale		-28.5		1.52	n.d.
AR08AS27	21.1	Siltstone	Disappear *Bositra* sp.		-29.0	0.91	n.d.
AR08AS99	19.9	Tuff					n.d.
AR08AS26	19.8	Black shale		-28.9		1.97	n.d.
AR08AS25	19.0	Black shale		-28.7		3.04	n.d.
AR08AS24	18.3	Black shale		-28.0		2.58	n.d.
AR08AS23	17.9	Siltstone			-29.3	1.07	n.d.
AR08AS22	17.7	Black shale		-27.5		1.55	n.d.
AR08AS21	17.5	Tuff					n.d.
AR08AS20	17.4	Black shale		-28.6		1.81	n.d.
AR08AS19	16.3	Black shale		-28.0		2.99	n.d.
AR08AS18	15.5	Black shale		-27.9		3.02	n.d.
AR08AS17	14.5	Black shale		-29.2		2.12	n.d.
AR08AS16	13.8	Tuff					n.d.
AR08AS15	13.7	Black shale		-28.3		2.29	1.60
AR08AS14	13.0	Tuff ?					n.d.
AR08AS13	12.7	Shale		-27.6		1.83	n.d.
AR08AS12	12.3	Siltstone			-28.0	0.87	n.d.
AR08AS11	11.9	Black shale		-26.8		1.84	n.d.
AR08AS10	10.9	Black shale		-29.8		1.66	n.d.
AR08AS98	10.1	Siltstone			-28.8	1.32	n.d.
AR08AS97	9.9	Shale		-27.1		1.63	n.d.
AR08AS96	9.7	Siltstone			-28.6	1.54	n.d.
AR08AS95	9.4	Black shale		-27.1		2.04	n.d.
AR08AS94	9.3	Siltstone			-28.3	2.13	n.d.
AR08AS93	9.1	Black shale		-26.7		2.72	n.d.
AR08AS92	9.0	Siltstone			-26.9	1.04	n.d.
AR08AS91	8.8	Tuff					n.d.
AR08AS90	8.7	Shale		-23.4		1.59	n.d.
AR08AS09	8.6	Siltstone			-27.4	1.32	n.d.
AR08AS08	8.4	Shale	Appear *Bositra* sp.	-28.3		0.89	n.d.
AR08AS07	6.6	Black shale	Start of Excursion	-28.8		1.57	n.d.
AR08AS06	6.0	Limestone			-28.7	0.65	n.d.
AR08AS05	5.0	Siltstone		-23.8		0.53	n.d.
AR08AS04	3.5	Limestone			-24.9	0.28	n.d.
AR08AS03	3.3	Shale		-22.5		1.35	n.d.
AR08AS02	2.4	Shale		-22.4		0.49	1.71
AR08AS01	0.6	Limestone			-25.2	0.08	n.d.

A total of 99 samples (~150 kg) were collected for petrographic and geochemical analyses. In the following paragraphs we describe the results of the lower 65 m of the logged section that contains the units of interest.

The sampled interval includes uppermost Pliensbachian beds of the ammonite *Fanninoceras disciforme* Assemblage Zone [= upper part of the *Fanninoceras* Assemblage Zone (Riccardi, 1984; Riccardi et al., 1990, 2000) equivalent to the Spinatum Standard Zone of Europe (Riccardi, 2008)]. The *Fanninoceras disciforme* Assemblage Zone partially coincides with the Andean bivalve *Radulonectites sosneadensis* Assemblage Zone (Damborenea, in Riccardi et al., 1990), which in the Serrucho Creek region matches the uppermost part of the Puesto Araya Formation (*sensu* Giambiagi et al., 2008). The Toarcian beds are recorded in the Tres Esquinas Formation in beds belonging to the ammonite *Dactylioceras hoelderi* Assemblage Zone (Riccardi, 2008), equivalent to the Serpentinum Standard Zone of Europe (Riccardi, 2008) and to the Andean bivalve *Posidonotis cancellata* Assemblage Zone (Damborenea, in Riccardi et al., 1990). As stated by Riccardi (2008), the earliest Toarcian *Dactylioceras tenuicostatum* Assemblage Zone, equivalent to the Tenuicostatum Standard Zone of Europe, marks a non-diversity peak in the ammonite record of the Andean region, and has not yet been recorded in the Serrucho Creek area.

3.2. Carbon analyses

Organic carbon isotopes were measured on 57 samples at the Institute for Energy Technology (IFE) at Kjeller, Norway. The bulk sediment samples were ground and 50 mg of powder was treated with 5 ml portions of 2 N HCl for decarbonation. This process was repeated until no more CO_2 was released. The samples were then cleaned with portions of 5 ml distilled water until neutral pH was reached and then dried in an oven at 80 °C overnight. The samples were weighed and approximately 5 mg was transferred to 9×15 mm tin capsules. The combustion of the samples was done in the presence of O_2 and Cr_2O_3 at 1700 °C with a Carlo Erba NCS 2500 element analyser. Water was removed on a chemical trap of $Mg(ClO_4)_2$ before separation of N_2 and CO_2 on a 2 m Poraplot Q GC column. Carbon content (wt.%) was quantified on the basis of the Thermal Ionization Detector results from the GC. The CO_2 was directly injected on-line to a Micromass Optima, Isotope Ratio Mass Spectrometer for determination of $\delta^{13}C$. To establish of a two point calibration line, USGS24 and an internal reference graphite were analysed together with the samples. Results are reported in δ notation, as per-mil (‰) deviation relative to the VPDB standard (Table 1). The precision for $\delta^{13}C$ is 0.1‰ (2 sigma).

Vitrinite was measured at IFE with a Zeiss MPM 03 photometer microscope equipped with an Epiplan-Neofluar 40/0.90 oil objective, after treating the samples with hydrochloric and hydrofluoric acid and polishing. Attempts to extract palynomorphs were unsuccessful as the organic matter was altered, as indicated by the vitrinite results (Table 1).

The total organic carbon (TOC) contents were measured on 57 powdered samples (Table 1) by oxidation of organic matter to CO/CO_2 between 300 and 650 °C with a LECO CR-412 at the Department of Geosciences of the University of Oslo.

3.3. Zircon dating

Zircons were extracted by disaggregating the unconsolidated tuff samples with a mortar and pestle, followed by slowly floating and decanting the clayey component and concluded by heavy liquid (Diiodomethane) separation. Two of the samples in the key interval of the section contained abundant populations of zircon with homogeneous appearance in terms of typology, elongation and morphology, whereas other samples contained few grains, partly subrounded and

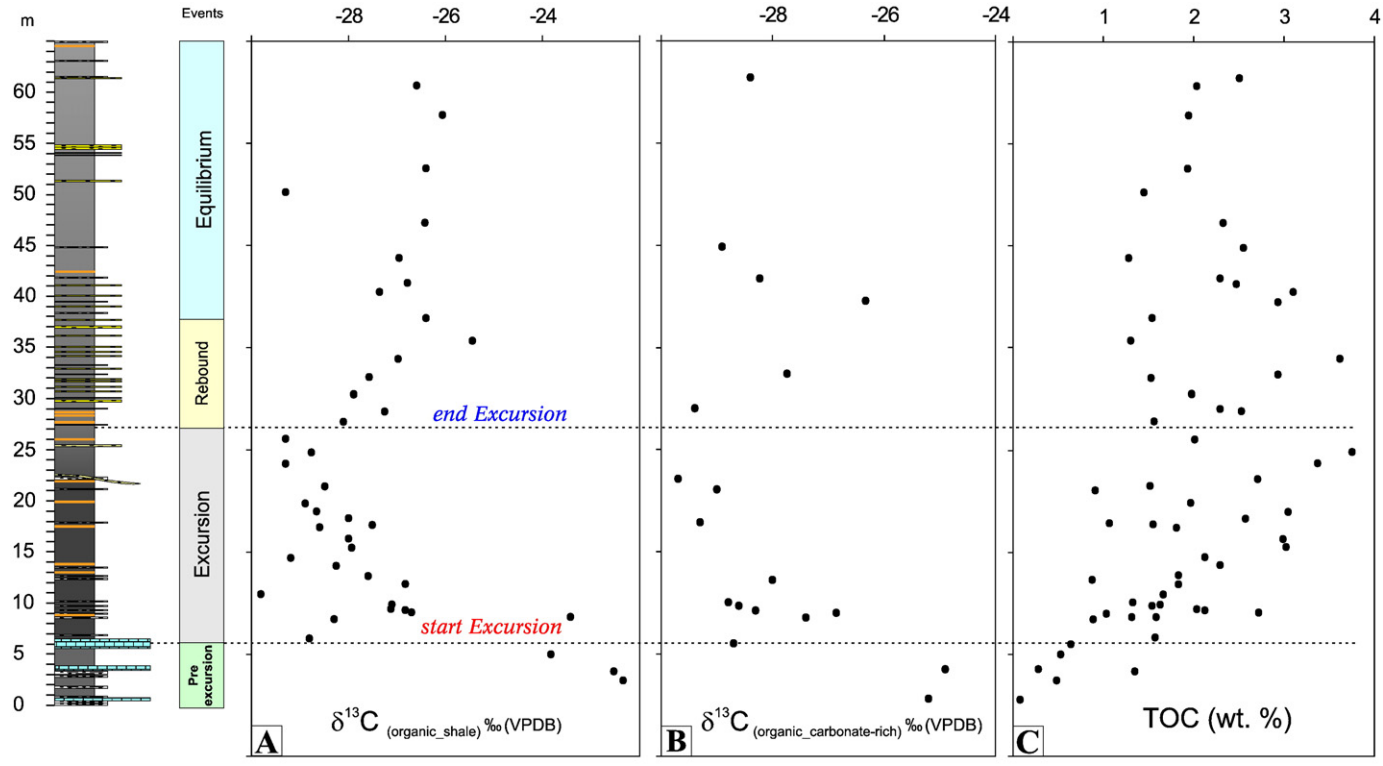

Fig. 6. Composite lithology log with the curves of isotope analyses of organic carbon in shale intervals (A), carbonate-rich layers (B) and total organic content (C). Both isotopic curves show an abrupt decrease coinciding with the occurrence of black shales. Low isotopic values persist through the interval with abundant black shales and *Bositra*. Higher up the values gradually increase stabilizing above ~35 m. The TOC curve reveals the opposite behaviour with gradually increasing values during the inferred TOAE and a progressive decrease in carbon content towards the upper part of the section. Horizontal dashed lines indicate the interpreted start and end of the CIE. These boundaries are consistent with field data and geochemical analyses. An interpretative log of the events, based on combined field and geochemistry observations, is also given.

likely of detrital origin. No useful data could be recovered from these latter samples. The best zircon grains were handpicked and abraded, either mechanically (see Krogh, 1982) or chemically (see Mattinson, 2005), and analysed by ID-TIMS following a modified procedure of Krogh (1973); details of the routines in the Oslo laboratory are given in Corfu (2004). The ages are calculated using the decay constants of Jaffey et al. (1971), regressing the data with the program Isoplot (Ludwig, 2003).

4. Results

4.1. The Pliensbachian–Toarcian section at Serrucho Creek

Pliensbachian and Toarcian sedimentary rocks are well exposed at the Serrucho Creek locality. The whole section dips gently (~20 °) towards the NE (Fig. 4). Here we present the lithological and biostratigraphical features of the three main units of the logged section (Fig. 5).

The stratigraphically lowest unit (0–6.5 m) represents the uppermost part of the Puesto Araya Formation. These fossil-rich lithologies consist of alternating fossiliferous limestones, carbonaceous silty units and shaly intervals, deposited in a stormy environment. Bivalves such us *Radulonectites sosneadensis* (Weaver), *Weyla (W.) bodenbenderi* (Behr.), *Kolymonectes coloradoensis* (Weaver), *Cucullaea rothi* (Leanza), *Isognomon jupiter* (Leanza), *Frenguelliela tapiai* (Lambert) and *Myophorella* sp. indet. were observed. Brachiopods such as *Rhynconelloidea cuyana* (Manceñido) and *Spiriferina* sp. were also recognised. Elsewhere in the Neuquén Basin the above mentioned fossils are associated with gastropods, serpulids, articulated crinoid stems and solitary corals (*Montlivaltia*) (see Damborenea and

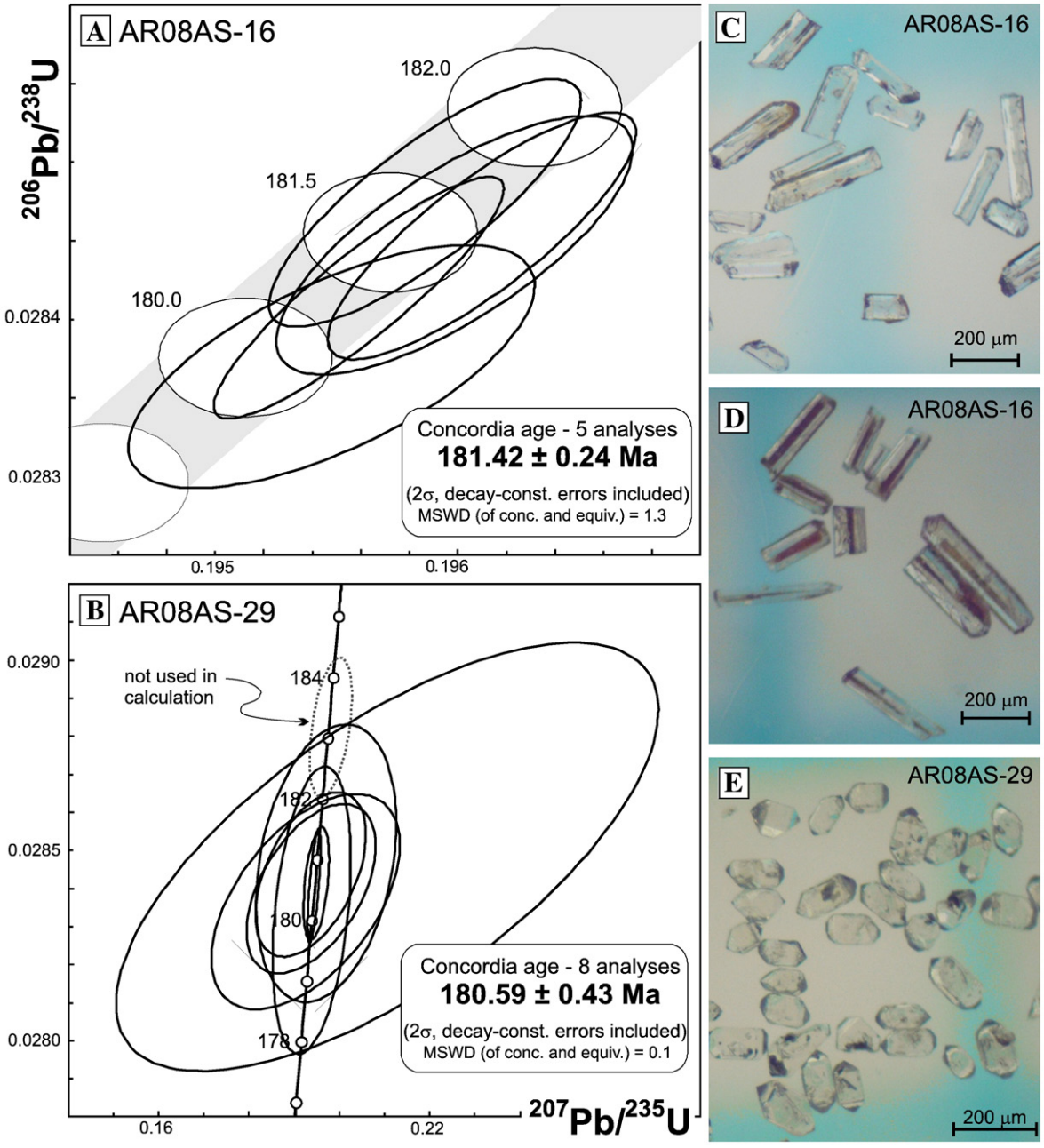

Fig. 7. (A) and (B): Concordia plots for zircon in the two tuffs at 13.8 and 21.9 m, respectively. Ellipses indicate the 2σ uncertainty. The grey concordia band and white age ellipses indicate the uncertainty in the decay constants. These are no longer visible in (B) due to the different scale of the plot. (C) and (D): Typical long-prismatic zircon crystals in AR08AS-16, with rusty cavities and longitudinal inclusions in (D). (E) Characteristic short prismatic zircon crystals from sample AR08AS-29. MSWD = mean square of weighted deviates.

Manceñido in Gulisano and Gutiérrez Pleimling, 1995). This invertebrate fauna forms part of the *Radulonectites sosneadensis* Assemblage Zone (Damborenea in Riccardi et al., 1990), indicating the proximity to the Pliensbachian/Toarcian boundary.

The second unit (6.5–29.5 m) defines the beginning of the Tres Esquinas Formation and its base marks the first appearance of black shale (Figs. 4B, C). The black shale dominates the unit, although thin (up to10 cm thick) intervals of carbonaceous siltstone and seven tuff layers are locally present. Particularly relevant for understanding the depositional environment is the appearance of the bivalve *Bositra* at the base of this unit. This genus is able to live for short periods in low-oxygenated waters (<0.6 ml of O_2/l of H_2O) within usually suboxic (O_2<0.1 ml O_2/l of H_2O) bottom waters (Brett and Baird, 1986; Savdra et al., 1991). The abundance of this bivalve increases towards the top of this unit forming shell pavements within the shale. The interval between 20 and 22.2 m shows a rapid decrease, and eventually disappearance, of this genus. Between 22.2 and 29.5 m the shales become gradually lighter in colour.

The third unit (29.5–65 m) mainly consists of grey shales interbedded with carbonate-rich siltstones and fine grained sandstones. The sandstone layers, particularly abundant between 30 and 41 m, were deposited in a turbiditic regime. Occasional sand injections in the lower unit (Fig. 5) are also observed. Five thin tuffaceous intervals were found in this unit. The ammonite *Hildaites* cf. *murleyi* (Moxxon) was recognised at 64 m, confirming that the shale still belongs to the Early Toarcian Stage (*Dactylioceras hoelderi* Assemblage Zone, equivalent to Serpentinum Standard Zone; see Riccardi, 2008).

4.2. Isotopes and total organic carbon

Carbon isotope analyses of the bulk organic carbon show that the $\delta^{13}C$ values of the shales cluster between −22.3 and −23.8‰ in the first 5 m (the Puesto Araya Formation). At 6.6 m there is an abrupt decrease in $\delta^{13}C$, which then fluctuates between −26.7 and −29.8‰ until 26.1 m. Organic matter in the shallower sediments reveal a gradual increase in $\delta^{13}C$ which, above 37.9 m remains between −26.4 and −26.6‰ all the way to 65 m. We have thus identified a negative carbon isotope excursion in the lower part of the studied section (Fig. 6A) The negative $\delta^{13}C$ excursion is recorded in the bulk organic matter from the carbonate-rich siltstones as well (Fig. 6B).

The TOC data show a progressive increase from 0.8 wt.% at the base of the section to a maximum of 3.75 wt.% at 24.8 m. At higher stratigraphic levels the TOC declines gradually (Fig. 6C).

Overall, the lithological characteristics, the isotope data, and the TOC measurements, show that the Early Toarcian carbon isotope excursion and anoxic event were recorded in the Serrucho Creek shales. In the following we organize the results in four "event zones" that can be correlated to other Early Toarcian sections: 1) *Pre-excursion zone* (0–6 m) characterized by the most positive $\delta^{13}C$ values, the lowest TOC content, and fossiliferous limestones; 2) The *anoxic event zone* (6–26.1 m) with a negative $\delta^{13}C$ excursion recorded in bulk organic matter, high TOC contents and black shales; 3) *Rebound zone* (26.1–37.9 m) defined by gradually increasing $\delta^{13}C$ values, disappearance of *Bositra*, appearance of sandstones layers and grey shales; and 4) *Equilibrium zone* (37.9–65 m) where the $\delta^{13}C$ values reach a plateau-like background value and the TOC content decreases.

4.3. Zircon dating and age estimations

Sample AR08AS-16 (13.8 m) yielded a population of uniform, relatively large, long prismatic zircon crystals (Fig. 7C). Longitudinal rusty cavities and inclusions of other minerals (e.g. biotite, and other unidentified phases) are however common (Fig. 7D). Five analyses yield overlapping data that define a Concordia age of 181.42 ± 0.24 Ma (Table 2; Fig. 7A).

The second sample AR08AS-29 (21.9 m) also provided a good selection of zircons with a dominant homogeneous morphology. In this case the crystals were short-prismatic to equant (Fig. 7E), and in general smaller, with less U and higher Th/U (1.5 to 2.6 vs. 0.6 to 0.9 in the above sample; Table 2). Because of the smaller size and lower Pb and U content the individual analyses are also less precise than in the previous sample. Eight analyses provide a Concordia age of 180.59 ± 0.43 Ma, not considering one data point plotting above the cluster (Fig. 7B). This data point (above the cluster) is presumably due to an inherited component.

Table 2
U–Pb data for zircon.

Zircon characteristics[a]	Weight[b]	U[b]	Th/U[c]	Pbc[d]	$^{206}Pb/^{204}Pb$[e]	$^{207}Pb/^{235}U$[f]	±2σ	$^{206}Pb/^{238}U$[f]	±2σ	rho	$^{207}Pb/^{206}Pb$[f]	±2σ	$^{206}Pb/^{238}U$[f]	±2σ	$^{207}Pb/^{235}U$[f]	±2σ
	(μg)	(ppm)		(pg)			(abs)		(abs)			(abs)	(Ma)			
AR08AS-16 tuff, 13.8 m																
lp cr in CA [12]	35	217	0.85	2.2	6101	0.1959	0.0005	0.02857	0.00006	0.83	0.04971	0.00008	181.6	0.4	181.6	0.4
lp CA [12]	17	240	0.71	1.0	7277	0.1961	0.0005	0.02855	0.00006	0.84	0.04981	0.00007	181.5	0.4	181.8	0.4
lp A [10]	5	966	0.63	2.3	3846	0.1960	0.0006	0.02855	0.00007	0.74	0.04979	0.00010	181.4	0.4	181.7	0.5
lp in CA in [12]	40	246	0.73	1.4	12,507	0.1956	0.0005	0.02851	0.00006	0.90	0.04975	0.00005	181.2	0.4	181.4	0.4
lp A [4]	8	421	0.87	2.4	2469	0.1955	0.0007	0.02847	0.00006	0.66	0.04980	0.00013	181.0	0.4	181.3	0.6
AR08AS-29C tuff, 21.9 m																
sp in CA [4]	2	184	2.21	1.7	404	0.1983	0.0039	0.02882	0.00015	0.44	0.04991	0.00089	183.2	0.9	183.7	3.3
sp A [1]	1	28	1.78	1.6	49	0.2109	0.0489	0.02848	0.00046	0.69	0.054	0.012	181.0	2.9	194	40
sp CA [1]	1	194	2.27	6.7	70	0.1973	0.0126	0.02847	0.00030	0.29	0.0503	0.0031	180.9	1.9	183	11
sp A [2]	1	157	2.42	1.9	165	0.1939	0.0100	0.02844	0.00018	0.49	0.0495	0.0024	180.8	1.1	180.0	8.4
sp in A [6]	12	121	2.58	1.5	1789	0.1947	0.0012	0.02841	0.00012	0.69	0.04971	0.00022	180.6	0.8	180.6	1.0
sp CA [4]	5	78	3.32	1.0	688	0.1952	0.0023	0.02841	0.00012	0.43	0.04983	0.00053	180.6	0.8	181.1	2.0
sp A [1]	1	55	1.49	0.8	144	0.1941	0.0117	0.02840	0.00018	0.50	0.0496	0.0028	180.5	1.1	180.1	9.9
sp A [1]	1	37	1.87	0.8	102	0.1928	0.0170	0.02836	0.00023	0.53	0.0493	0.0041	180.3	1.5	179	14
sp in CA [6]	10	32	2.58	4.4	146	0.1942	0.0070	0.02834	0.00031	0.34	0.0497	0.0017	180.2	1.9	180.2	6.0

[a] Z = sp = short prismatic (l/w = 2–4); lp = long prismatic (l/w = >4); cr = fractured; in = inclusions; A = mechanical abrasion; CA = chemical abrasion; [N] = number of grains in fraction; abs = absolute value.
[b] Weight and concentrations are known to be better than 10%, except for those near the ca. 1 μg limit of resolution of the balance.
[c] Th/U model ratio inferred from 208/206 ratio and age of sample.
[d] Pbc = total common Pb in sample (initial + blank).
[e] Raw data corrected for fractionation.
[f] Corrected for spike contribution, fractionation, blank (lab average: 6/4 = 18.3 (2%), 7/4 = 15.555 (1%), 8/4 = 2.056 (2%)) and initial common lead (as calculated from Stacey and Kramers, 1975) using uncertainties of 2% for 6/4 and 8/4 and 1% for 7/4); uncertainties are calculated by propagating the main sources of uncertainty (do not include the uncertainty of the spike, estimated of <0.2% based on calibration with various reference solutions).

We use the two measured ages and the assumption of a constant sedimentation rate to extrapolate linearly the ages for the beginning and the end of the negative carbon isotope excursion. The uncertainties of the extrapolated ages were estimated by Monte Carlo simulations, with 10,000 pairs of random replicates from normal distributions with the given radiometric means and 2-sigma error bars. The modelling gave ages of 182.16 ± 0.6 Ma (at 6.6 m) for the beginning of the excursion and 180.16 ± 0.66 Ma for the end (at 26.1 m), thus constraining the duration of the 19.5 m of the anoxic event to between 0.74 and 3.26 Ma. (Fig. 8)

5. Discussion

5.1. Depositional environment and the CIE

Several changes in the depositional environment are recorded in the studied section. The lowermost 6.5 m contains predominantly fossiliferous limestones indicative of warm marine water conditions, consistent with the northernmost location of South America during Pliensbachian–Toarcian times (Iglesia Llano, 2008). The $\delta^{13}C$ data show the highest values (up to −22.3‰) and the lowest TOC content (0.08%) in this interval.

The sediments above 6.5 m are characterized by a change in the trend of TOC and $\delta^{13}C$. Carbon isotope values abruptly decrease and TOC contents rapidly increase. Increasing TOC contents together with ^{13}C-depleted organic matter are characteristic of the Toarcian anoxic shales (e.g. Jenkyns, 1988; Cohen et al., 2007). Additionally, the presence of black shales with *Bositra* between 6.5 and 22.2 m strengthens the interpretation that this interval contains the TOAE. No significant lithological changes are recorded in the section between 6.5 and 30 m except for the gradual lightening in colour of the shales and the presence of two thin sandstone beds injected from the units located above 30 m. This suggests that the recorded carbon isotopic excursion, and in particular the rebound observed in the $\delta^{13}C$ curve, reflect a global signal and are not caused by local or regional changes in the depositional environment.

Although our sampling resolution is limited, it is interesting to compare the Serrucho Creek section with northern hemisphere

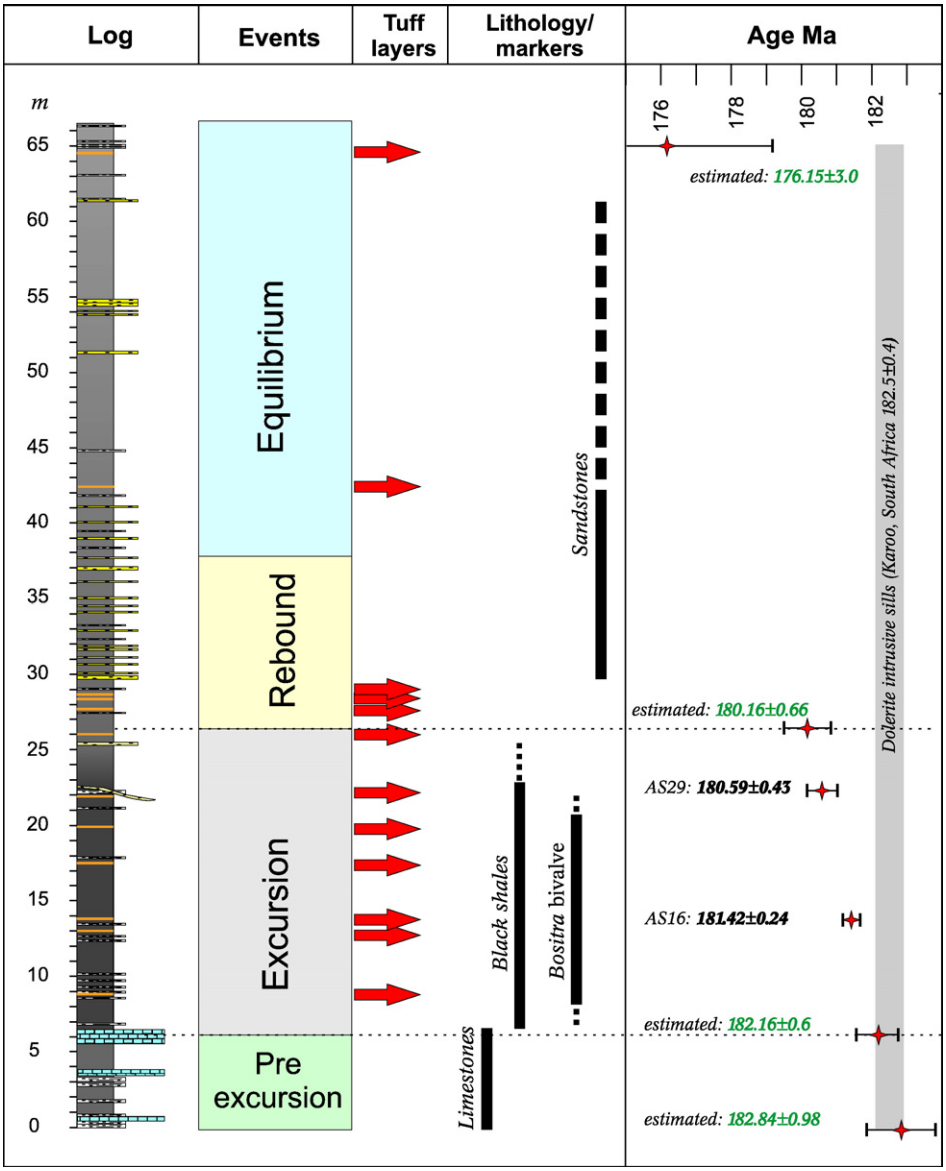

Fig. 8. Lithology log with an interpretation of the different units based on combined field and analytical results. The four units (pre-excursion, excursion, rebound, and equilibrium) are defined by the carbon isotope variations. The presence of the key lithologies and fossil markers is indicated by vertical black lines. The tuff layers are marked by red arrows. The dating of two of these layers within the TOAE gave values of 180.59 ± 0.43 Ma and 181.42 ± 0.24 Ma, respectively. Assuming a constant sedimentation rate, the beginning of the CIE is estimated at 182.17 ± 0.6 Ma. This value is within the age obtained from the dolerite sills in the Karoo Basin, South Africa (Svensen et al., 2007).

sections. Littler et al. (2010) provide a detailed description of sections from Peniche (Portugal) and Yorkshire (UK). In addition to the TOAE, these sections reveal an earlier and sharp negative carbon isotope excursion occurring at the Pliensbachian–Toarcian boundary. We cannot exclude the presence of this excursion in the Serrucho Creek section. Our results show that a ^{13}C-depletion up to −28.7‰ is already present in the fossiliferous limestones at 6 m and that, after an initial spike at the Pliensbachian-Toarcian boundary, a slight decrease in the ^{13}C-depletion can be inferred in both shale and carbonate-rich lithologies in the first 10 m (Fig. 6). We can also not exclude the presence of two separate excursions at Serrucho Creek, however such differentiation would be too speculative considering the sample spacing. Based on the available data it is thus not possible to establish if the negative carbon isotope excursion documented by Littler et al. (2010) at the Pliensbachian–Toarcian boundary, can also be considered a southern hemisphere event.

The remaining part of our logged section (i.e., 30–65 m) is characterized by gradual changes. This section marks the appearance of turbiditic sandstones which become more dominant towards the top. Here, organic carbon is less abundant and more enriched in ^{13}C. Similar lithological changes are recorded at other localities in the Neuquén Basin. For instance, an intra-Toarcian unconformity within the Los Molles Formation in the southern Neuquén Basin is characterized by the superposition of two different foraminifera zones separated by a depositional hiatus (Angelozzi in Vergani, 2005). Also, the Early Toarcian in the lower Los Molles Formation was still influenced by extensional processes (Gómez Omil et al., 2002; Verzi et al., 2005), but the subsequent oblique convergence contributed to change the tectonic pattern of the basin (Silvestro and Zubiri, 2008). These geological changes can possibly also explain the fact that the organic matter above 35 m has δ^{13}C values significantly lower (~−26.5‰) than those recorded before the anoxic event (~−22.5‰).

5.2. Dating

The accuracy of Mesozoic zircon U–Pb ages is mainly controlled by geological factors and the calibration of the U–Pb tracer. Geological factors include effects due to inheritance of older Pb and due to Pb loss. Loss of Pb can be minimized by selecting the most appropriate zircon grains and treating them with mechanical or chemical abrasion. The absence of a geological bias is difficult to prove in individual cases, but is commonly evaluated based on the consistency of repeated analyses. The U–Pb tracer can be calibrated against known solutions and then checked by measuring well characterized reference solutions or zircons. Measurements of the Earthtime 100 Ma solution with our spike yields an average (8 values) that is about 1‰ below that obtained with the ET535 tracer solution prepared by the Earthtime Initiative (see www.earth-time.org). Our spike calibration translates into a potential bias of less than 0.2 Ma, which is below the precision of our ages. This type of uncertainties and limitations shows some of the discrepancies that can arise.

There is no international agreement defining the age of the boundary between the Toarcian and the Pliensbachian stages. The widely used estimate of 183 ± 1.5 Ma is based on ammonoid biostratigraphy but was not ratified in the most recent stratigraphic charts (Gradstein et al., 2004; Ogg et al., 2008). However, this age is in agreement with Pálfy (2008) that sets the boundary at 183.6 ± 1.7–1.1 Ma by interpolating between a U–Pb zircon age for the Early (?) Pliensbachian and another for the Late Bajocian. Thus the date is indirect and subject to some degree of uncertainty. Our estimate of the Pliensbachian–Toarcian boundary (182.16 ± 0.6 Ma) is younger than the one proposed by Pálfy (2008), the difference being larger than the potential bias from the spike mentioned above. Also important in this respect is the fact that both our field and regional observations did not show evidence of hiatuses in the Serrucho Creek and did not highlight significant changes in the depositional environment during the inferred TOAE. Thus our precise zircon ages can safely be extrapolated to the beginning and end of the TOAE layers assuming a constant sedimentation rate. Hence, given the good quality of the two zircon populations in our samples, the internal consistency of the analyses, the satisfactory calibration of our spike, and the thorough field observations, we are confident that our date is more robust than the extrapolated value of Pálfy (2008).

Several authors have attempted to estimate the duration of the TOAE. Jenkyns (1988) suggested a general span of about 500 ky. This value has later been refined to ~600 ky, excluding the rebound period, and almost 1 Ma including the rebound (McArthur et al., 2000; Suan et al., 2008). Cohen et al. (2007) propose a duration of 200 ka (300 ka including the rebound). Our results constrain its duration to between 0.74 and 3.26 Ma excluding the rebound and including the possible precursor peak described by Littler et al. (2010).

5.3. Karoo Basin degassing and the TOAE

Svensen et al. (2004) proposed a new model to explain the Paleocene Eocene Thermal Maximum (PETM), showing that more than 700 hydrothermal vent complexes in the North East Atlantic formed as the result of magmatic intrusions in organic-rich sediments. These intrusions caused rapid maturation and eventually triggered the release of methane to the atmosphere. The same mechanism has also been proposed to explain the TOAE by invoking a high flux of thermogenic methane released from baked organic-rich shale during sill emplacement in the Karoo Basin (Svensen et al., 2004, 2007) and from metamorphism of coal in Antartica (McElwain et al., 2005).

Identification of the isotopic and TOC excursion at the Pliensbachian–Toarcian boundary in the Serrucho Creek section and the ages provided by the tuff deposits from the neighbouring Andean volcanic arc, support the hypothesis that thermogenic methane is a plausible trigger for the initial phase of the TOAE (Svensen et al., 2007). Our age (Fig. 8) of the beginning of the CIE (182.16 ± 0.6 Ma) overlaps the age of intrusive sills in the Karoo Basin within error (182.5 ± 0.4 Ma, see Svensen et al., 2007). We highlight that both the U–Pb ages from the Serrucho Creek and the Karoo Basin were measured with the same method in the same laboratory (i.e. Department of Geosciences, University of Oslo) and are thus directly comparable.

As also pointed out by Cohen et al. (2007), we suggest that other feed back processes proposed by other authors (e.g. dissociation of gas hydrates, e.g. Hesselbo et al., 2000; Kemp et al., 2005) could represent the second step of further release of isotopically light carbon to the atmosphere.

6. Conclusions

We present new geological and geochemical data of shales from the Neuquén Basin, Argentina, showing that the Toarcian Oceanic Anoxic Event is recorded in the southern hemisphere. Interbedded tuff layers have successfully been dated by the U–Pb method on zircons. We conclude that:

- Field observations reveal distinct lithological (black shales) and paleontological (*Bositra*) evidences of an anoxic environment.
- Chemostratigraphy in the same interval shows a negative carbon isotope excursion in bulk rock organic matter, with a drop of δ^{13}C up to ~−8‰ demonstrating the presence of the TOAE.
- Based on U–Pb zircon dating of newly discovered tuff layers, ages of 182.16 ± 0.6 Ma and 180.16 ± 0.66 are extrapolated for the beginning and the end of the CIE respectively, constraining the duration to between 0.74 and 3.26 Ma. The lower estimate is considered the most realistic considering other published estimates.
- The age calculated for the beginning of the CIE matches the U–Pb zircon age of sill intrusions in the Karoo Basin (182.5 ± 0.4 Ma), supporting the hypothesis that the thermogenic methane released

from the Karoo Basin resulted in the Toarcian carbon cycle perturbations.
- A new and improved dating of the Pliensbachian–Toarcian boundary (182.16 ± 0.6 Ma) is provided.

Acknowledgements

The editor R. Carlson, A. Schimmelmann and two anonymous reviewers are thanked for their constructive reviews. This study was supported by a *Centre of Excellence grant* to PGP, and by a *Young Outstanding Researcher* grant (180678/V30) to H. Svensen, both of them from the Norwegian Research Council. The authors would like to thank C. Portilla (Dirección General de Minería, Zapala), A. Garrido (Zapala Museo Olsacher), O. Galland (PGP) and the authorities of SEGEMAR for their support during the fieldwork. We are grateful to Ø. Hammer (PGP) for his help during Monte Carlo simulations and M. Roscher (PGP) for providing Toarcian palaeogeography.

References

Brett, E., Baird, G.C., 1986. Comparative taphonomy: a key to paleoenviromental interpretation of fossil preservation. Palaios 10, 597–616.
Cohen, A.S., Coe, A.L., Kemp, D.B., 2007. The Late Palaeocene–Early Eocene and Toarcian (Early Jurassic) carbon isotope excursions: a comparison of their time scales, associated environmental changes, causes and consequences. J. Geol. Soc. Lond. 164 (6), 1093–1108.
Corfu, F., 2004. U–Pb age, setting, and tectonic significance of the anorthosite–mangerite–charnockite–granite suite, Lofoten-Vesterålen, Norway. J. Petrol. 45, 1799–1819. doi:10.1093/petrology/egh034.
Damborenea, S.E., 1987. Early Jurassic bivalvia of Argentina. Part 2. Superfamilies Pteriacea, Buchiacea and part of Pectinacea. Palaeontographica (A), 199(4/6): 113–216.
Damborenea, S.E., Polubotko, I.V., Sey, I.I., Paraketsov, K.V., 1992. Bivalve zones and assemblages of the Circum-Pacif. In: Westermann, G.E.G. (Ed.), Jurassic of the Circum-Pacific. University of Cambridge Press, pp. 300–307.
Giambiagi, L., Bechis, F., Lanés, S., Tunik, M., García, V., Suriano, J., Mescua, J., 2008. Formación y evolución Triásico–Jurásica del depocentro Atuel, Cuenca Neuquina, provincial de Mendoza. Revista de la Asociación Geológica Argentina. Simposio Jurásico de América del Sur 63 (4), 52–53.
Giambiagi, L., Suriano, J., Mescua, J., 2005. Extensión multiepisódica durante el Jurásico temprano en el depocentro Atuel de la Cuenca Neuquina. Revista de la Asociación Geológica Argentina 60 (3), 524–534.
Gómez Omil, R.G., Schmithalter, J., Cangini, A., Albariño, L. and Corsi, A., 2002. El Grupo Cuyo en la Dorsal de Huincul: consideraciones estratigráficas, tectónicas y petroleras, Cuenca Neuquina, 5º Congreso de Exploración de Hidrocarburos, Mar del Plata.
Gradstein, F.M., Ogg, J.G., Smith, A.G., 2004. A Geologic Time Scale 2004. Cambridge University Press.
Groeber, P., 1946. Observaciones geológicas a lo largo del meridiano 70° 1. Hoja Chos Malal. Revista de la Sociedad Geológica Argentina 1 (3), 177–208.
Gulisano, C.A., Gutiérrez Pleimling, A., 1995. Field guide: the Jurassic of the Neuquén Basin. b) Mendoza province. Asociación Geológica Argentina 3 1–103 Serie E.
Gulisano, C.A., Gutierrez Pleimling, A., Digregorio, R.E., 1984. Esquema estratigráfico de la secuencia jurásica del oeste de la provincia del Neuquén, 9° Congreso Geológico Argentino. Actas 1. Buenos Aires 236–259.
Hermoso, M., Le Callonnec, L., Minoletti, F., Renard, M., Hesselbo, S.P., 2009. Expression of the Early Toarcian negative carbon-isotope excursion in separated carbonate microfractions (Jurassic, Paris Basin). Earth Planet. Sci. Lett. 277 (1–2), 194–203.
Hesselbo, S.P., Grocke, D.R., Jenkyns, H.C., Bjerrum, C.J., Farrimond, P., Morgans Bell, H.S., Green, O.R., 2000. Massive dissociation of gas hydrate during a Jurassic oceanic anoxic event. Nature 406 (6794), 392–395.
Hesselbo, S.P., Jenkyns, H.C., Duarte, L.V., Oliveira, L.C.V., 2007. Carbon-isotope record of the Early Jurassic (Toarcian) Oceanic Anoxic Event from fossil wood and marine carbonate (Lusitanian Basin, Portugal). Earth Planet. Sci. Lett. 253 (3–4), 455–470.
Iglesia Llano, M.P., 2008. Paleogeografía de América del Sur durante el Jurásico. Revista de la Asociación Geológica Argentina. Simposio Jurásico de América del Sur 63 (4), 499–501.
Jaffey, A.H., Flynn, K.F., Glendenin, L.E., Bentley, W.C., Essling, A.M., 1971. Precision measurement of half-lives and specific activities of 235U and 238U. Phys. Rev. C: Nucl. Phys. 4, 1889–1906.
Jenkyns, H.C., 1988. The early Toarcian (Jurassic) anoxic event; stratigraphic, sedimentary and geochemical evidence. Am. J. Sci. 288 (2), 101–151.
Kemp, D.B., Coe, A.L., Cohen, A.S., Schwark, L., 2005. Astronomical pacing of methane release in the Early Jurassic period. Nature 437 (7057), 396–399.
Krogh, T.E., 1973. A low contamination method for hydrothermal decomposition of zircon and extraction of U and Pb for isotopic age determinations. Geochim. Cosmochim. Acta 37, 485–494.
Krogh, T.E., 1982. Improved accuracy of U–Pb zircon ages by the creation of more concordant systems using an air abrasion technique. Geochim. Cosmochim. Acta 46, 637–649.
Küspert, W., 1982. Environmental change during oil shale deposition as deduced from stable isotope ratios. In: Einsele, S., Seilacher, A. (Eds.), Cyclic and Event Stratification. Springer-Verlag, Berlin, pp. 482–501.
Lanés, S., 2005. Late Jurassic to early Jurassic sedimentation in northern Neuquén Basin, Argentina. Tectosedimentary evolution of the first trangression. Geologica Acta 3 (2), 81–106.
Legarreta, L., Gulisano, C.A., 1989. Análisis estratigráfico de la Cuenca Neuquina (Triásico Superior–Terciario Inferior). In: Chebli, G.A., Spalletti, L.A. (Eds.), Cuencas Sedimentarias Argentinas. Instituto Miguel Lillo, Universidad Nacional de Tucumán. Serie Correlación Geológica 6, San Miguel de Tucumán, pp. 221–244.
Legarreta, L., Uliana, M.A., 1999. El Jurásico y Cretácico de la Cordillera Principal y la Cuenca Neuquina. 1. Facies sedimentarias. In: Caminos, R. (Ed.), Geología Argentina. : Servicio Geológico Minero Argentino. Instituto de Geología y Recursos Minerales, Buenos Aires, pp. 399–432.
Littler, K., Hesselbo, S.P., Jenkyns, H.C., 2010. A carbon-isotope perturbation at the Pliensbachian–Toarcian boundary: evidence from the Lias Group, NE England. Geol. Mag. 147 (2), 181–192.
Ludwig, K.R., 2003. Isoplot 3.0. A geochronological toolkit for Microsoft Excel, Berkeley Geochron. Center Spec. Publ. No. 4, p. 70.
Manceñido, M.O., 1990. The succession of Early Jurassic brachiopod faunas from Argentina: correlations and affinities. In: MacKinnon, D.I., Lee, D.E., Campbell, J.D. (Eds.), Brachiopods through Time. A.A. Balkema, Rotterdam, pp. 397–404.
Mattinson, J.M., 2005. Zircon U–Pb chemical abrasion ("CA-TIMS") method: Combined annealing and multi-step partial dissolution analysis for improved precision and accuracy of zircon ages. Chem. Geol. 220 (1–2), 47–66.
Mattioli, E., Pittet, B., Suan, G., Mailliot, S., 2008. Calcareous nannoplankton across the Early Toarcian Anoxic Event: implications for paleoceanography within the western Tethys. Paleoceanography 23, PA3208. doi:10.1029/2007PA001435, 2008.
McArthur, A.G., Algeo, T.J., Van de Schootbrugge, B., Li, Q., Howarth, R.J., 2008. Basinal restriction, black shales, Re–Os dating, and the Early Toarcian (Jurassic) oceanic anoxic event. Paleoceanography 23, PA4217. doi:10.1029/2008PA001607, 2008.
McArthur, J.M., Donovan, D.T., Thirlwall, M.F., Fouke, B.W., Mattey, D., 2000. Strontium isotope profile of the early Toarcian (Jurassic) oceanic anoxic event, the duration of ammonite biozones, and belemnite palaeotemperatures. Earth Planet. Sci. Lett. 179 (2), 269–285.
McElwain, J.C., Wade-Murphy, J., Hesselbo, S.P., 2005. Changes in carbon dioxide during an oceanic anoxic event linked to intrusion into Gondwana coals. Nature 435 (7041), 479–482.
Ogg, J.G., Ogg, G., Gradstein, F.M., 2008. The Concise Geologic Time Scale. Cambridge University Press.
Pálfy, J., 2008. The quest for refined calibration of the Jurassic time-scale. Proc. Geol. Assoc. 119 (1), 85–95.
Ramos, V.A., 1988. The tectonics of the central Andes: 30° to 33° S latitude. In: S. Clark and D. Burchfield (Editors), Processes in continental lithospheric deformation. Geol. Soc. Am. Spec. Pap. 31–34.
Ramos, V.A., 2000. Evolución tectónica de la Argentina. In: Caminos, R. (Ed.), Geología Argentina. Instituto de Geología y Recursos Minerales, Anales, pp. 715–784.
Ramos, V.A., 2009. Anatomy and global context of the Andes: main geologic features and the Andean orogenic cycle. Geological Society of America Memoir 204, 31–65.
Riccardi, A.C., 1984. Las asociaciones de amonitas del Jurásico y Cretácico de la Argentina. 9 Congreso Geológico Argentino. Actas 4, 559–595.
Riccardi, A.C., 2008. El Jurásico de la Argentina y sus amonites. Revista de la Asociación Geológica Argentina. Simposio Jurásico de América del Sur 63 (4), 625–643.
Riccardi, A.C., Damborenea, S.E., Manceñido, M.O., 1990. Lower Jurassic of South America and Antarctic Peninsula. In: G.E.E. Westermann and A.C. Riccardi (Editors), Jurassic taxa ranges and correlation charts for the Circum Pacific. Newsl. Stratigr. 75–103.
Riccardi, A.C., Leanza, H.A., Damborenea, S.E., Manceñido, O.M., Ballent, S.C., Zeiss, A., 2000. Marine Mesozoic biostratigraphy of the Neuquén Basin. Zeitschrift für Angewandte Geologie, SH 1 (2000), 102–108.
Savdra, C.E., Bottjer, D.J., Seilacher, A., 1991. Redox-related benthic events. In: Einsele, G., Ricken, W., Seilacher, A. (Eds.), Cycles and events in stratigraphy. Springer-Verlag, Berlin, pp. 324–341.
Schouten, S., van Kaam-Peters, H.M.E., Rijpstra, W.I.C., Schoell, M., Sinninghe Damste, J.S., 2000. Effects of an oceanic anoxic event on the stable carbon isotopic composition of Early Toarcian carbon. Am. J. Sci. 300 (1), 1–22.
Silvestro, J., Zubiri, M., 2008. Convergencia oblicua: modelo estructural alternativo para la Dorsal Neuquina (39º S), Neuquén. Revista de la Asociación Geológica Argentina 63 (1), 49–64.
Stacey, J.S., Kramers, J.D., 1975. Approximation of terrestrial lead isotope evolution by a two-stage model. Earth Planet. Sci. Lett. 34, 207–226.
Stipanicic, P.N., 1969. El avance en los conocimientos del Jurásico Argentino a partir del esquema de Groeber. Revista de la Asociación Geológica Argentina 24 (4), 367–388.
Suan, G., Pittet, B., Bour, I., Mattioli, E., Duarte, L.V., Mailliot, S., 2008. Duration of the Early Toarcian carbon isotope excursion deduced from spectral analysis: consequence for its possible causes. Earth Planet. Sci. Lett. 267 (3–4), 666–679.
Svensen, H., Planke, S., Chevallier, L., Malthe-Sørenssen, A., Corfu, F., Jamtveit, B., 2007. Hydrothermal venting of greenhouse gases triggering Early Jurassic global warming. Earth Planet. Sci. Lett. 256 (3–4), 554–566.
Svensen, H., Planke, S., Malthe-Sørenssen, A., Jamtveit, B., Myklebust, R., Eidem, T., Rey, S.S., 2004. Release of methane from a volcanic basin as a mechanism for initial Eocene global warming. Nature 429, 542–545.
Uliana, M.A., Biddle, K.T., 1988. Mesozoic–Cenozoic paleogeographical and geodynamic evolution of southern South America. Rev. Bras. Geocienc. 18, 172–190.

Valencio, S.A., Gagnoni, M.C., Ramos, A.M., Riccardi, A.C., Panarello, H.O., 2005. Chemostratigraphy of the Pliensbachian, Puesto Araya Formation (Neuquén basin). Argentina. Geologica Acta 3 (2), 147–154.

van de Schootbrugge, B., McArthur, J.M., Bailey, T.R., Rosenthal, Y., Wright, J.D., Miller, K.G., 2005. Toarcian oceanic anoxic event: an assessment of global causes using belemnite C isotope records. Paleoceanography 20, PA3008. doi:10.1029/2004PA001102.

Vergani, G.D., 2005. Control estructural de la sedimentación jurásica (Grupo Cuyo) en la Dorsal de Huincul, Cuenca Neuquina. Modelo de falla lístrica rampa-plano invertida. Boletín de Informaciones Petroleras 1 (1), 32–42.

Vergani, G.D., Tankard, A.J., Belotti, H.J., Welsink, H.J., 1995. Tectonic evolution and paleogeography of the Neuquén Basin, Argentina. American Association of Petroleum Geologists, Memoir, Tulsa 62, 383–402.

Verzi, H., Raggio, M.E., Suárez, M., 2005. Volume interpretation of a turbidite system, Los Molles Formation, Neuquén Basin, Argentina. In: Soubies, D., Arteaga, M., Fantín, F. (Eds.), La sísmica de reflexión más allá de la imagen estructural: 5° Congreso de Exploración de Hidrocarburos, Actas, Mar del Plata, pp. 219–226.

Volkheimer, W., 1978. Descripción geológica de la Hoja 27a, Cerro Sosneado. Servicio Geológico Nacional, Boletín 151 Buenos Aires, 83 pp.

Weaver, C., 1931. Paleontology of the Jurassic and Cretaceous of west central Argentina, 1. Memoir University of Washington, Seattle. 1-469.

Wignall, P.B., Hallam, A., Newton, R.J., Sha, J.G., Reeves, E., Mattioli, E., Crowley, S., 179–190, 2006. Jurassic extinction in Tibet. An eastern Tethyan (Tibetan) record of the Early Jurassic (Toarcian) mass extinction event. Geobiology 4. doi:10.1111/j.1472-4669.2006.00081.

Wignall, P.B., Newton, R.J., Little, C.T.S., 2005. The timing of paleoenvironmental change and cause-and-effect relationships during the early Jurassic mass extinction in Europe. Am. J. Sci. 305 (10), 1014–1032.